P2.54 OBSERVATIONS OF THE IMPACT OF OROGRAPHIC CUMULUS CLOUDS ON THE AMBIENT FLOW

Yonggang Wang* and Bart Geerts
University of Wyoming

1. INTRODUCTION

The role of cumulus convection in the climate system remains a significant challenge as moist convection operates on a range of scales, a significant portion of which is sub-gridscale for climate models. Thus Cu parameterizations have been developed to represent the effect of sub-gridscale convection on the profile of resolved variables, in particular temperature, humidity, and momentum. Resolved variables change in part in response to detrainment of water and energy from Cu clouds into their cloud-free environment. Several observational Cu studies have examined the effect of lateral and vertical mixing between cloudy and clear air on the dynamics and microphysics of Cu clouds (e.g., Blyth 1993; Small and Chuang 2008). The terminology for the mixing process between cloudy and clear air distinguishes between an *entrainment* event, which takes place in cloud, and a *detrainment* event, which evolves outside the cloud edge.

The effect of detraining cloudy air on the surrounding clear air has been studied mainly using numerical simulations. For instance, Bretherton and Smolarkiewicz (1989) use a two-dimensional numerical model to study convectively-generated subsidence, gravity waves, and turbulent detrainment. They conclude that detrainment is largely governed by the local vertical gradient of buoyancy in cloud: if the buoyancy of a parcel decreases with height, then its lower part is accelerated faster than the upper region, and this induces divergence and detrainment. Taylor and Baker (1991) confirm this conclusion using soundings and aircraft-inferred lateral mass fluxes across the cloud edge, but again they do not depict resulting changes in the environment. Other modeling studies include Carpenter et al. (1998a), who use a three-dimensional cloud model and show that significant detrainment at mid levels is often caused by collapsing Cu turrets, and De Rooy and Siebesma (2008), who use a large-eddy simulation model to study the parameterization of detraining shallow Cu clouds.

The present study examines the patterns of detrainment and decay downwind of orographic convection. Aircraft in-situ data, airborne mm-wavelength radar data, fixed-source time lapse photography, and close-proximity radiosonde data are used to examine how orographic Cu clouds alter the environment within the layer of Cu development. The target clouds are relatively shallow (~2 km depth), so that they do not produce precipitation and convective downdrafts, which would alter the boundary layer.

2. DATA SOURCES

This study uses data collected on 8 August 2006 in the Cumulus Photogrammetric, In-situ and Doppler Observations (CuPIDO-06) campaign (Damiani et al. 2008). Fig. 1 shows CuPIDO-06 instrument layout around the Santa Catalina Mountains, a relatively isolated mountain range about 25 km in diameter in southeast Arizona, peaking about 2 km above the surrounding plains. On this day a large number of non-precipitating orographic Cu clouds were penetrated by an instrumented aircraft, the University of Wyoming King Air (WKA), which carried a 95 GHz (3.2 mm) Doppler radar, the Wyoming Cloud Radar (WCR), with fixed (non-scanning) antennas pointing up (zenith), down (nadir), and slant-forward (Damiani et al. 2008).

A series of M-GAUS (Mobile GPS Advanced Upper-air Sounding) radiosondes was launched at 30 minute intervals during the 8 August WKA flight, from a location called Windy Point, on the southeast side of

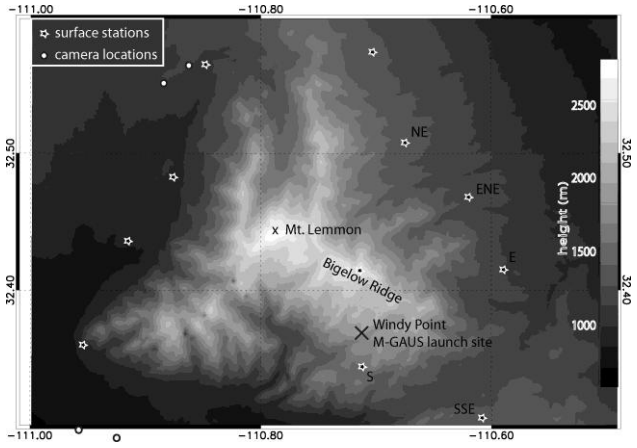

Fig. 1: Terrain map of the Santa Catalina Mountains in south-eastern Arizona, showing CuPIDO-06 measurement sites. The city of Tuscon stretches across the plains in the lower left of the image.

* *Corresponding author address*: Yonggang Wang, Department of Atmospheric Science, University of Wyoming, Laramie, WY 82071, USA; email: wyg@uwyo.edu

the mountain (Fig. 1). The prevailing lower-tropospheric wind was east-southeasterly on 8 August, thus the radiosonde data described the airmass upstream of the mountain. Each radiosonde ascended in clear air at about 5-10 km upstream of the target orographic Cu clouds. We verified that none of the nine radiosondes penetrated clouds at any level.

Ten integrated surface flux facility (ISFF) stations were positioned in the foothills around the Santa Catalina Mountains during CuPIDO-06 (Fig. 1). These stations recorded meteorological measurements at five minute intervals. Data from the ISFF stations on the east-southeast side of Mt. Lemmon are used to describe the inflow feeding the orographic Cu, and data from downwind ISFF stations are used to examine the effect of orographic convection on the convective boundary layer (CBL), e.g. cooling by convective downdrafts and/or cloud shading.

Two cameras on the southwest side of the mountain (Fig. 1) enable stereo-photogrammetric analysis (Zehnder et al. 2007). The time lapse camera animations, at a time resolution of 20 seconds, nicely illustrate the movement and evolution of Cu clouds over the Santa Catalina Mountains. The stereo-photogrammetric data are used here to track the cloud top height of the deepest Cu cloud.

Flight-level thermodynamic and cloud variables are calculated, for instance the wet equivalent potential temperature (θ_q), and the total water mixing ratio (r_{TOT}). These variables require temperature, mixing ratio, pressure, cloud liquid water content (LWC) and ice water content (IWC). The LWC is inferred from the Forward Scattering Spectrometer Probe (FSSP), by integrating over all droplet size bins (Brenguier et al. 1994). The IWC is ignored because ice was essentially absent on all flight legs examined herein. The static pressure measurement on the WKA is accurate within ~0.3 hPa, except in vigorous Cu clouds, where the accuracy deteriorates to ~1.0 hPa.

Flight-level temperature is measured by a reverse flow thermometer, an immersion probe with an accuracy of 0.5 K in clear air. The reverse flow housing was designed to minimize sensor wetting in cloud, but the comparison between cloud entrance and cloud exit composite temperature traces shows that some probe wetting does occur, and thus also evaporative cooling following the aircraft's exit from cloud (Wang and Geerts 2009). In the present study, the temperature has been corrected for this sensor's evaporative cooling bias following Wang and Geerts (2009).

Flight-level humidity is inferred from a chilled-mirror dewpoint sensor, which has an adequate accuracy (1 K) but a slow response time. To a first order, the response of this instrument to a step-function change is an exponential adjustment, reaching the actual dewpoint after about 30 seconds, corresponding with flight track distance of 2.5 km, which is larger than most cloud widths. For derived variables dependent on humidity, we have to assume in-cloud saturation and slowly varying conditions outside cloud, as measured by the chilled-mirror dewpoint sensor. Because of the slow response of this sensor, we cannot depict an accurate fine-scale detrainment signature immediately outside cloud, within 2.5 km from the cloud edge. Thus we focus on the turn-around loop tracks flown on opposite sides of the orographic convection. By design these leg-end loops were not started until at least 30 seconds after exiting a cloud.

Finally, we use radiosonde wind data and flight-level vertical and horizontal air velocities. The latter are derived from the WKA gust probe using an established procedure (Lenschow et al. 1991).

3. RESULTS

3.1 Case selection

The 8 August 2006 case was chosen for this study for several reasons. Firstly, convection was confined to the mountain footprint and was not too shallow (resulting in an insignificant detrainment signal) nor too deep, as lightning poses a hazard to the WKA. Secondly, the air was relatively dry above the CBL, making detrainment patterns more detectable. Thirdly, the wind was fairly weak at all levels of Cu development (<7 m s^{-1} in all nine soundings), and rather uniform with height, so that convective towers readily formed over the mountain, without being significantly sheared. Fourthly, numerous flight tracks were flown along the mean wind direction, from the east (between 90-110°), which allows us to contrast the upstream side with the downstream side of the region of surface-driven Cu convection. The aircraft documented the upwind and downwind regions of the Cu clouds well, because of the 180° turns with a rather large radius of curvature.

Time lapse photography indicates that shallow orographic Cu first developed near Mt. Lemmon at 1603 UTC. Successive Cu towers developed at the eastern side of the Santa Catalina Mountains and drifted towards the west with the prevailing wind. Cu clouds generally formed and drifted along the narrow spine of Bigelow Ridge (Fig. 1), which happens to be aligned with the prevailing wind. The convective towers were clearly age-ordered from east to west and generally decayed west of Mt. Lemmon. The maximum cloud top height never grew to the equilibrium level of 13-14 km MSL, inferred from the 1730-1830 UTC M-GAUS profiles. Instead, convection was capped at about 8 km MSL, except for one tower that reached a height of 9.1 km at 1950

UTC (Fig. 2a). The WCR-inferred cloud tops were generally lower than the camera-inferred ones. The WKA flew a series of legs aligned with Bigelow Ridge between 1656-1925 UTC, i.e. before local solar noon. No precipitation shafts were apparent in the time lapse photography during this period.

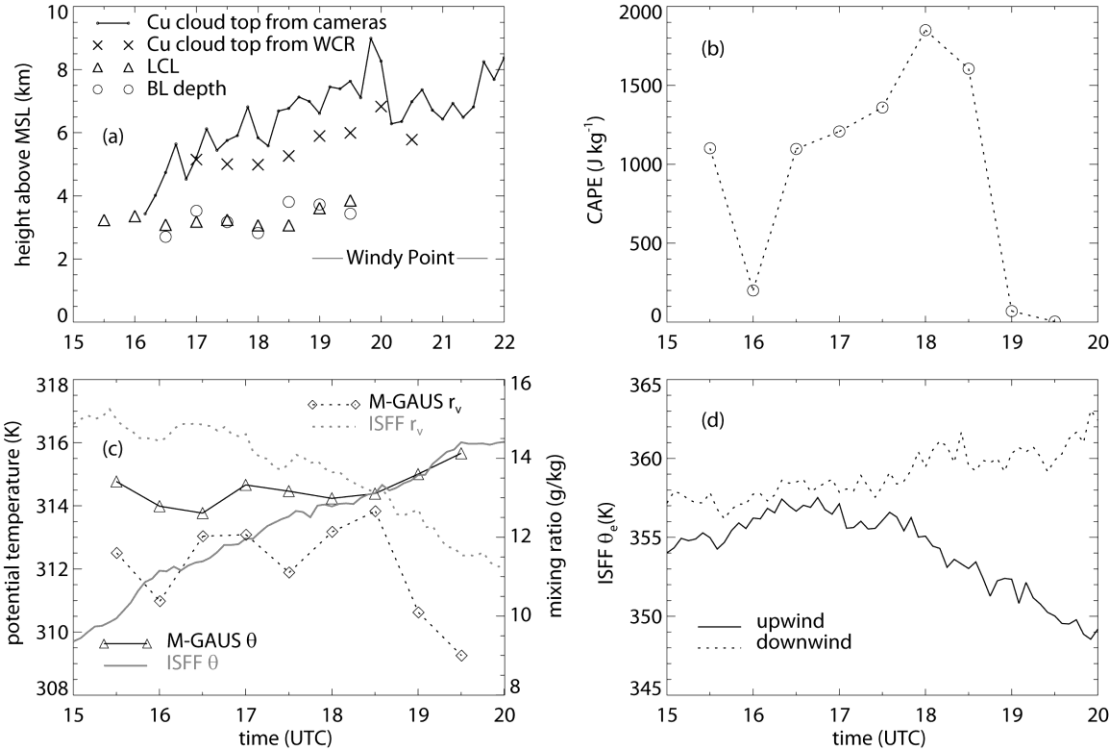

Fig. 2: Evolution of (a) the cloud base (LCL), the mixed layer depth, and highest top of Cu over the Santa Catalina Mountains, (b) mixed-layer CAPE (mixing depth: 50 hPa), (c) BL and surface (ISFF) potential temperature and mixing ratio and (d) equivalent potential temperature (θ_e) from ISFF stations. The data are inferred from the M-GAUS soundings, ISFF stations, stereo-photogrammetric data, and WCR reflectivity profiles.

3.2 Evolution of the boundary layer

We now examine the evolution of temperature and humidity near the surface and in the CBL along the upwind foothills of the mountain, and the resulting change in convective available potential energy (CAPE), in order to understand the observed evolution of Cu tops. It appears that the first M-GAUS radiosonde (at 1530 UTC, 4 hours before local solar noon) was launched before the CBL top reached Windy Point, a rather sharp terrain outcropping about 1.2 km above the Tucson valley. The CBL deepened above the elevation of Windy Point shortly after 1530 UTC, and above Mt. Lemmon (about 2.0 km above the valley) during the course of the morning to a maximum depth of 3.6 km MSL at 1830 UTC (Fig. 2a).

Five stations, labeled NE, ENE, E, SSE, and S in Fig. 1, are used to describe the average upwind conditions at the surface. The flow at these stations was generally anabatic, with an average anabatic component (defined in Demko et al. 2009) of 1.8 m s^{-1} during the WKA flight. The average surface potential temperature (θ) at the five stations generally increased, and the mixing ratio (r_v) decreased during the flight (Fig. 2c).

We use the M-GAUS soundings to compute the mean θ and r_v in a layer 100-600 m above Windy Point. They confirm an increase in θ, although by only 1-2 K, as opposed to nearly 6 K according to ISFF data for the same period (Fig. 2c). The first three M-GAUS soundings suggest a decrease in CBL θ, but this apparent cooling is because in the first two soundings the CBL top had not reached 600 m above Windy Point level. In fact the 100-600 m AGL layer above Windy Point was 4 K warmer (in terms of θ) than at the surface over the eastern foothills at 1530 UTC (Fig. 2c). This apparent stratification weakened gradually and disappeared by 1800 UTC.

The BL humidity trend before 1830 UTC is not clear: the soundings suggest a slight increase in r_v, in

disagreement with ISFF data (Fig. 2c). Both data sources agree on rapid drying between 1830-1930 UTC, resulting in an increase in the lifting condensation level (LCL) (Fig. 2a) and a decrease in CAPE values. The sounding-based mixed-layer CAPE decreased from over 1,500 J kg^{-1} at 1830 UTC to under 100 J kg^{-1} half an hour later (Fig. 2b). The upwind surface θ_e started to decrease an hour earlier (Fig. 2d). This lower θ_e may have mixed in the deep CBL and may have been advected over the mountain, reducing the CAPE there. The cloud top height trend lags by over one hour: a decline in maximum cloud top height started only at 1950 UTC (Fig. 2a). Some of this delay is simply due to the time needed to advect the drier air over Mt Lemmon, located 12 km downwind of Windy Point.

It is unlikely that the decrease in CAPE after 1800 UTC is a consequence of orographic convection, which may cause surface cooling and possibly moistening, by cloud shading and convective downdrafts. Instead a warming and drying trend is observed (Fig. 2c). The BL above Windy Point is also unlikely to have been affected by the convection, given the persistent easterly flow. Even the downwind ISFF stations appear to have remained unaffected by convection over the Santa Catalina Mountains: θ_e steadily increased there, due to warming, not moistening (Fig. 2d).

It is remarkable that the high CAPE values at 1800-1830 UTC and the lack of convective inhibition (CIN < 50 J kg^{-1}; as evident also in the steady growth of Cu convection, Fig. 2a) did not result in deep convection over the mountain. Deep convection did break out around 1915 UTC over the mountain range just (~45 km) east of the Santa Catalina Mountains, resulting in a dense anvil that advected over the Santa Catalina Mountains between 2015-2130 UTC. The resulting shading, and the low-level advection of a patch of dry air, apparently suppressed deep convection over the Santa Catalina Mountains at a time when thunderstorms broke out over every other high mountain in the vicinity.

3. 3 Evolution of static stability

The M-GAUS soundings are used to examine changes in static stability above the BL. A persistent stable layer just below 7 km MSL (Fig. 3a) apparently capped Cu convection on this day. This stable layer gradually lowered by about 400 m from the first to the

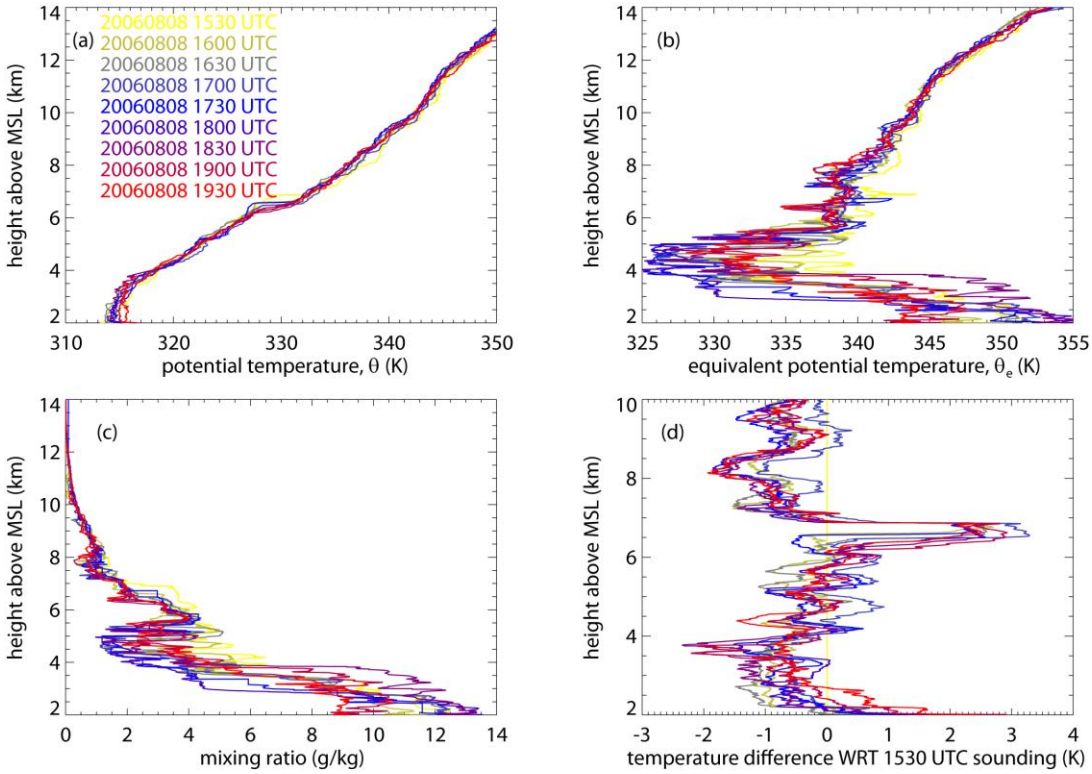

Fig. 3: Changes in thermodynamic profiles between 1530-1930 UTC on 08/08/2006: (a) θ, (b) θ_e, (c) mixing ratio, (d) temperature difference with respect to the first sounding at 1530 UTC.

last M-GAUS sounding, and it weakened during this period. This weakening is due to warming of the base of the stable layer at ~6.5 km MSL, mainly early during this period (Fig. 3d). The cause of this ~3 K warming, larger than any warming in the CBL, is not detrainment from convection: most of the warming occurred when Cu towers still topped out well below this level (Fig. 2a). Rather the most likely cause is local subsidence, as the mixing ratio decreased in this layer (Fig. 3c). This subsidence could be a gravity wave response to lower-level orographic convection.

A persistent relatively moist layer was present between ~5.2 – 6.6 km, below the stable layer (Fig. 3c). Time lapse photography indicates that a thin layer of altostratus was present in the morning. This layer had mostly evaporated by 1530 UTC. The CBL was quite moist (except in the last two soundings), whereas the air above was much drier (Fig. 3c), resulting in strong potential instability, mainly between 2.5-4.5 km MSL. This is the layer in which Cu clouds grew over the mountain. The main flight level was at 4.5 km MSL. The large decrease in θ_e between 2.5 km MSL and this flight level (Fig. 3b) increases the probability of detecting a signal of detrainment from rather benign Cu clouds.

3.4 Flight-level Cu detrainment/decay patterns

We now analyze combined flight-level and remotely-sensed WKA measurements and M-GAUS sounding data for WKA flight sections consisting of a straight leg over the mountain, and two loops, one at each end of the straight leg. Fig. 4 shows one example of the combined analysis for the WKA flight

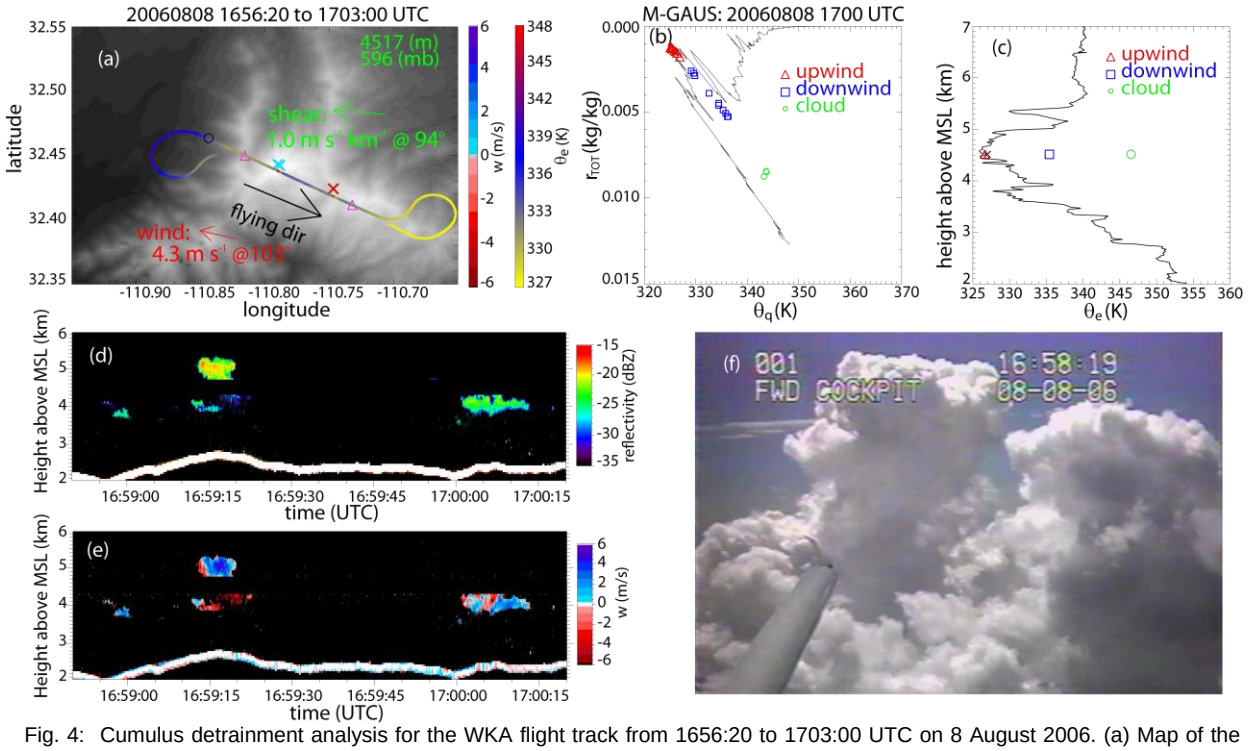

Fig. 4: Cumulus detrainment analysis for the WKA flight track from 1656:20 to 1703:00 UTC on 8 August 2006. (a) Map of the flight track, colored by θ_e over a terrain map (grayscale, with white representing the elevation of Mt. Lemmon, 2791 m). Also shown is the flight-level vertical air velocity (colored crosses, displaced slightly north of the track). The flight level for this track is listed in the upper right corner in green, in MSL height and pressure units. The large black arrow indicates the flight direction. The mean flight-level wind (red vector) and wind shear (green vector) are inferred from the nearest-in-time M-GAUS sounding released at Windy Point, and are computed over the depth of the Cu (cloud base to top). (b) Paluch diagram showing WKA cloud penetrations and out-of-cloud WKA data along the flight turns on the west (downwind) and east (upwind) sides of the orographic convection. Also shown is the nearest M-GAUS sounding. (c) Average θ_e values for the WKA turns on the downwind and upwind sides of the orographic convection, average θ_e value of the cloud penetrations, and M-GAUS θ_e profile. The flight level is indicated with a black cross on the M-GAUS profile in (b) and (c) (in this case the cross is hidden under the red triangles in b). (d) Vertical transect of WCR reflectivity above and below flight level for the straight portion of this track, between the pink triangles shown in (a); the flight level is the black belt (radar blind zone), and the mountain terrain can be seen below. (e) As in (c), but WCR vertical velocity. (f) Cu photo taken by a forward-pointing camera in the cockpit of the WKA at a time shown in the upper right corner from a location shown as a black circle on the flight track in (a).

track from 1656:20 to 1703:00 UTC on 8 August 2006. It first maps the WKA flight track and the Cu clouds encountered along this track (Fig. 4a). The flight-level gust probe vertical velocity in each penetrated cloud is shown in Fig. 4a as well. Next, the upstream environment is contrasted against the downstream environment, in terms of mapped θ_e patterns (Fig. 4a), a Paluch diagram (Fig. 4b), and a θ_e profile (Fig. 4c). The WCR reflectivity transect along the track (Fig. 4d) indicates cloud vertical structure. The vertical velocity profile of these clouds (Fig. 4e) qualitatively describes life cycle and level of divergence. And a photo from a forward-looking cockpit camera, shot at the beginning of the flight leg (Fig. 4f), illustrates the clouds' visual appearance. For the calculation of flight-level θ_e, it is assumed that the air is saturated in cloud (Section 2). The Paluch diagram in Fig. 4b is unconventional in that it analyses not only in-cloud observations, as is common practice (e.g., Paluch 1979; Carpenter et al. 1998b; Wang and Geerts 2009), but also flight-level data collected in the clear air either upstream or downstream of the orographic Cu. Both r_{TOT} and θ_q are conserved under pseudo-adiabatic moist processes (Paluch 1979).

In all chosen flight sections the mean flight-level wind is almost aligned with the flight leg orientation (118°), but slightly closer to easterly (97-112°). The turn-around loops at the end of each straight leg are displaced to the left of the straight legs however, so that they nicely cover an area upstream and downstream of the orographic convection. In each of the eight sections, the upwind (eastern) and downwind (western) loops were flown at the same pressure level. θ_e is highest in-cloud, and higher in the downwind loop than in the upwind loop. It also tends to be higher just down-track of clouds, which is an instrument bias (Section 2). The isolated patches of high θ_e air in the downwind loops, evident in panels (a) of Fig. 4 probably result from detrainment from existing Cu clouds, or, more likely, the debris of decayed orographic convection advected downstream.

The Paluch diagrams in panel (b) of Fig. 4 indicate that the upwind loop is relatively uniform, with θ_q and r_{TOT} values very close to the M-GAUS values at a corresponding altitude [shown as a black cross on the sounding line in Fig. 4b]. The fact that the [θ_q, r_{TOT}] properties of air in the downwind loop are more distinct from the environment (as measured by the upwind radiosonde) and more similar to cloudy air than air in the upwind loop suggests that the downwind airmass is substantially enriched with CBL air (Fig. 4b and Fig. 4c). The mean θ_e in the downwind loop corresponds with ambient θ_e values encountered ~0.5-2.0 km below flight level, although it remains much lower than the θ_e values in the CBL (Fig. 4c). The downstream enrichment signature is quite clear in this case study precisely because of the significant drop in θ_e from the CBL to flight level.

The properties of the downwind air are closer to those of the upwind environment than those within Cu clouds, indicating that both unmodified ambient air and former cloud material (detrained from cloud or cloud detritus) are sampled in the downwind loop. The linear alignment of [θ_q, r_{TOT}] values encountered along the downwind loop suggests different mixing fractions of these two sources of air. Downwind air parcels whose [θ_q, r_{TOT}] values are closer to the corresponding values in cloud than to those found upwind (described by sounding or upwind flight loop) originate mostly within the orographic Cu clouds (Fig. 4b). Note that the in-cloud [θ_q, r_{TOT}] values may be slightly overestimated because it is assumed that the cloudy air is saturated, which is not always the case. Relative humidity values under 100% are not uncommon in cloud, especially near the Cu cloud edge (Wang and Geerts 2010).

4. DISCUSSION

The hypothesis of moisture-convection feedback (or convective conditioning) states that the immediate environment of Cu clouds is modified by preceding convective towers such that Cu growth is facilitated, most likely by the moistening of the environment, which weakens the erosive effect of entrainment. This hypothesis was first examined in early numerical studies of entrainment and in laboratory experiments (Scorer 1957; Squires and Turner 1962; Warner 1970; Cotton 1975), and gained support amongst modelers aiming to capture the large-scale spatio-temporal characteristics of tropical oceanic deep convection (e.g., Randall and Huffman 1980; Grabowski and Moncrieff 2004; Derbyshire et al. 2004). To the authors' knowledge, this hypothesis has not been experimentally verified at the scale of individual Cu clouds.

There is little doubt that orographic convection enriched the environment with CBL air on 08/08/2006. In 16 of the 18 constant-elevation upwind-downwind loop pairs flown, θ_e was enhanced in the downwind loop (Fig. 5b). The θ_e enrichment generally was stronger at mid-levels (flight level 4.5 km MSL) than at higher levels (above 5 km MSL), because the ambient (upwind) θ_e reached a minimum near 4.5 km MSL (Fig. 3b). Another factor may be that θ_q of a Cu cloud tends to decrease due to the dry air entrainment into clouds, and thus the air detrained at higher levels is relatively depleted of BL θ_e.

This increase of θ_e near the level of minimum θ_e clearly decreased the lower-tropospheric potential

instability. It is quite possible that potential instability was further impeded by a decrease in θ_e in the CBL, as the decaying Cu convection on the west side of the mountain advected lower θ_e values down into the CBL. No convective downdrafts into the CBL were observed by the WCR however. The most significant downdrafts in decaying convection downwind of the mountain did not carry hydrometeors into the CBL. Clearly these Cu towers lacked the concentrations of hydrometeors needed to sustain a near-moist-adiabatic lapse rate resulting in even benign microbursts. Moreover, the downwind ISFF stations do not reveal any surface cooling or moistening that would be associated with convective downbursts. In fact surface θ_e values downstream of the mountain were higher than those upstream of the mountain and steadily increased during the orographic Cu growth period (Fig. 2d).

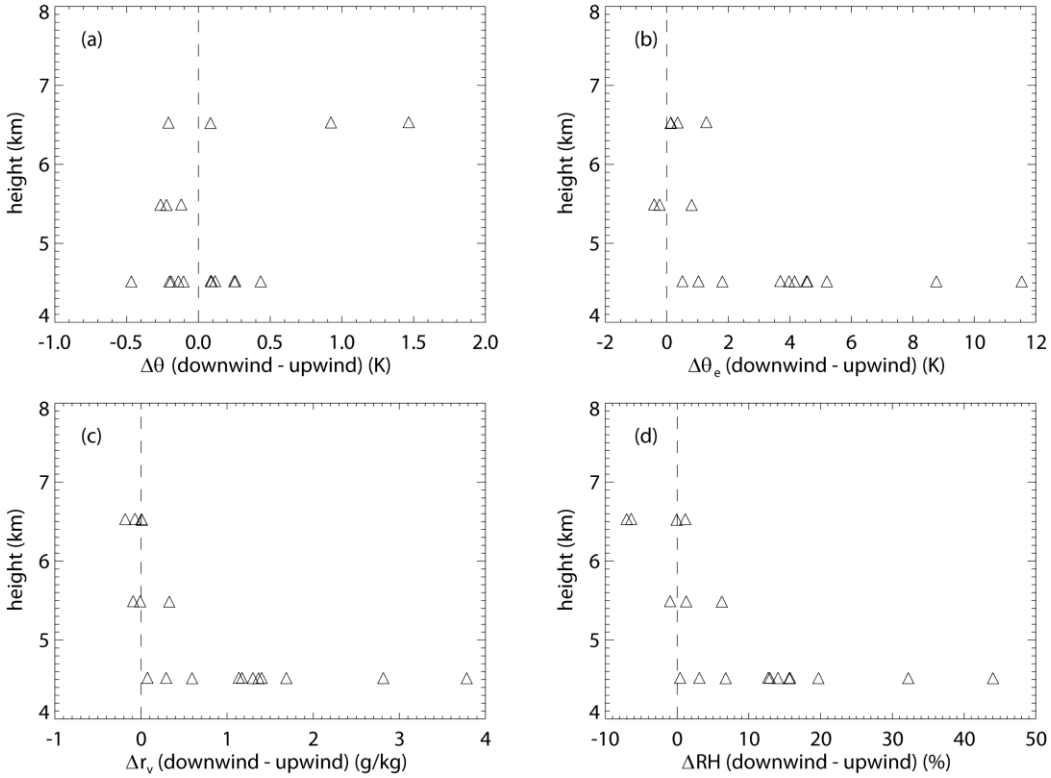

Fig. 5: Scatter plot of the average (a) θ difference, (b) θ_e difference, (c) r_v difference, and (d) relative humidity difference between downwind and upwind loops as a function of flight level, for all downwind-upwind loop pairs flown at constant flight level on 8 August 2006.

While potential instability decreased in the Cu cloud layer, the absolute and relative humidity generally increased in the downstream environment (Fig. 5c and d), especially at the lowest flight level, where the upwind environment was relatively dry (Fig. 3c). Clearly no new convection developed downstream of the orographic Cu simply because the air had been advected away from the "hot spot" over elevated terrain. But it is possible, in theory, that the successive deepening of the Cu towers over Mt. Lemmon was affected by moistening of the lower cloud layer by a series of shallow Cu growing upstream, over Bigelow ridge. This would serve as some confirmation of the moisture-convection feedback hypothesis. The time scale of advection over the hot spot (in particular, the 18 km along-wind distance over Bigelow Ridge towards Mt. Lemmon) is about 60-70 min, which is long compared to the life cycle of Cu *mediocris*. Time lapse photography and WCR sequences confirm that some Cu go through an entire lifecycle along Bigelow Ridge before reaching its western end. It is most likely that the gradual growth of the orographic Cu top between 1600-1800 UTC (before solar noon) can be explained simply by steady surface warming (Fig. 2c), leading to an increase in CAPE (Fig. 2b).

Still, the continued growth of the Cu towers over Mt. Lemmon, especially between 1800-1950 UTC (Fig. 2a) when the upstream CAPE rapidly declined, may have been facilitated by an increase in humidity between in the shallow Cu layer over Bigelow Ridge. Indeed some Cu appeared to grow over Mt. Lemmon

in the wake of decaying convection advected from the east on 8 August. Of course this could be a coincidence. Thus, while it is possible that successive Cu towers over Mt. Lemmon grew more readily in the humid debris of decaying Cu clouds, the significance of the moisture-convection feedback on Cu growth in this case cannot be proven.

5. CONCLUSIONS

In this study mainly three data sources, i.e. flight-level measurements, profiling cloud radar data and sounding data, collected as part of the CuPIDO-06 campaign over the Santa Catalina Mountains in Arizona, are combined to study the effect of non-precipitating orographic convection on the ambient air. The main conclusions are as follows:

- The environment downwind of Cu clouds erupting over a hot spot, such as a mountain, is clearly enriched with boundary-layer air. This enrichment is mainly the result of the decay of orographic convection, rather than detrainment *per se*. The enrichment in θ_e across the mountain is not an artifact of stratified flow over the mountain, as it is due not to an increase in θ, but rather an increase in humidity.
- The fraction of air originating from Cu clouds in air parcels downwind of the mountain can be estimated from a Paluch diagram showing the cloudy air, the upwind air, and the downwind air, all at the same level. Some air parcels, sampled 5-20 km downwind of the clouds, still mostly contain orographic cloud residue.
- This enrichment in θ_e reduces potential instability in the lower troposphere but convection also increases ambient humidity, thus it may render the downwind environment more conducive to penetrative convection. This mechanism (known as the moisture-convection feedback mechanism) does not explain the commonly observed gradual deepening of daytime convection over mountains since the mid-tropospheric plume of modified air usually is blown off the mountain before new convection can bubble up.

Acknowledgements: This work was supported by National Science Foundation (NSF) grants ATM-0444254 and ATM-0849225. We thank the crew of the University of Wyoming King Air for collecting the data and providing high-quality products for the CuPIDO-06 campaign. This paper benefitted from discussions with Wojciech Grabowski and Jeffrey French. The cloud top chronology was kindly provided by Joseph A. Zehnder.

References

Blyth, A.M., 1993: Entrainment in cumulus clouds. *J. Appl. Meteor.*, **32**, 626–641.

Brenguier, J., D. Baumgardner, and B. Baker, 1994: A review and discussion of processing algorithms for FSSP concentration measurements. *J. Atmos. Ocean. Tech.*, **11**, 1409–1414.

Bretherton, C. S., and P. K. Smolarkiewicz, 1989: Gravity waves, compensating subsidence and detrainment around cumulus clouds. *J. Atmos. Sci.*, **46**, 740–759.

Carpenter, R.L., K.K. Droegemeier, and A.M. Blyth, 1998a: Entrainment and Detrainment in Numerically Simulated Cumulus Congestus Clouds. Part II: cloud budgets. *J. Atmos. Sci.*, **55**, 3433–3439.

Carpenter, R.L., K.K. Droegemeier, and A.M. Blyth, 1998b: Entrainment and Detrainment in Numerically Simulated Cumulus Congestus Clouds. Part III: Parcel Analysis. *J. Atmos. Sci.*, **55**, 3440–3455.

Cotton, W.R., 1975: Theoretical cumulus dynamics. *Rev. Geophys. Space Sci,* **13**, 419-448.

Damiani, R., J. Zehnder, B. Geerts, J. Demko, S. Haimov, J. Petti, G.S. Poulos, A. Razdan, J. Hu, M. Leuthold, and J. French, 2008: Cumulus Photogrammetric, In-situ and Doppler Observations: the CuPIDO 2006 experiment. *Bull. Amer. Meteor. Soc.,* **89**, 57–73.

Demko, J. C., B. Geerts, J. Zehnder, and Q. Miao, 2009: Boundary-layer energy transport and cumulus development over a heated mountain: an observational study. *Mon. Wea. Rev. ,* **137**, 447–468.

Derbyshire, S.H., I. Beau, P. Bechtold, J.-Y. Grandpeix, J.-M. Piriou, and J.-L. Redelsperger, 2004: Sensitivity of moist convection to environmental humidity, *Quart. J. Roy. Meteor. Soc.,* **130**, 3055 – 3079.

De Rooy, W. C., and A. P. Siebesma, 2008: A simple parameterization for detrainment in shallow cumulus. *Mon. Wea. Rev.*, **136**, 560–576.

Grabowski, W. W., and M. W. Moncrieff, 2004: Moisture-convection feedback in the tropics. *Quart. J. Roy. Meteor. Soc.*, **130**, 3081-3104.

Lenschow, D., E. Miller, and R. Friesen, 1991: A three-aircraft intercomparison of two types of air motion measurement systems. *J. Atmos. Ocean. Tech.*, **8**, 41–50.

Paluch, I. R., 1979: The entrainment mechanism in Colorado cumuli. *J. Atmos. Sci*., **36**, 2467–2478.

Randall, D.A., and G.J. Huffman, 1980: A stochastic model of cumulus clumping. *J. Atmos. Sci.,* **37**, 2068–2078.

Scorer, R.S., 1957: Experiments on convection of isolated masses of buoyant fluid. *J. Fluid. Mech.*, **2**, 583-594.

Small, J.D., and P.Y. Chuang, 2008: New observations of precipitation initiation in warm cumulus clouds. *J. Atmos. Sci.*, **65**, 2972–2982.

Squires, P., and J. S. Turner, 1962: An entraining jet model for cumulonimbus updraughts. *Tellus,* **14**, 3422–3434.

Taylor, G. R., and M. B. Baker, 1991: Entrainment and detrainment in cumulus clouds. *J. Atmos. Sci.*, **48**, 112–121.

Wang, Y., and B. Geerts, 2009: Estimating the evaporative cooling bias of an airborne reverse flow thermometer. *J. Atmos. Ocean. Tech*., **26**, 3-21.

Wang, Y., and B. Geerts, 2010: Humidity variations across the edge of trade wind cumuli: observations and dynamical implications. *Atmos. Res*., in press. doi:10.1016/j.atmosres.2010.03.017.

Warner, J., 1970: On steady-state one-dimensional models of cumulus convection. *J. Atmos. Sci.,* **27**, 1035–1040.

Zehnder, J.A., J. Hu and A. Razdan, 2007: A stereo photogrammetric technique applied to orographic convection. *Mon. Wea. Rev*, **135**, 2265–2277.